Acta Metallurgica, Vol. 27, pp. 1765 to 1778

0001-6160/79/1101-1765$02.00/0

ON THE FORMATION AND INTERACTION OF SMALL METAL PARTICLES

A. R. THÖLÉN

Laboratory of Applied Physics I, Technical University of Denmark, Building 307, 2800 Lyngby, Denmark

(*Received* 21 *March* 1979; *in revised form* 4 *June* 1979)

Abstract—The formation, growth and interaction of small metal particles (10–100 nm) produced by gas evaporation has been studied. Single metal atoms diffuse radially out from the evaporation source until they condense at a temperature of roughly 0.35–0.40 T_m, where T_m is the absolute melting temperature. The particles then grow, mainly by coalescence. The final size of the particles is determined by evaporation temperature and gas pressure.

When the particles interact strong adhesion strain fields are created. These strain fields cause plastic deformation (twins) in many metals, but no twins were observed in aluminium and iron.

Résumé—Nous avons étudié la formation, la croissance et l'interaction de petites particules métalliques (10–100 nm) produites par évaporation. Les atomes métalliques diffusent individuellement et radialement à partir de la source d'évaporation et se condensent à une température de l'ordre de 0,35 à 0,40 T_m, où T_m est la température absolue de fusion. Les particules croissent ensuite, essentiellement par coalescence. La taille finale des particules est déterminée par la température d'évaporation et la pression du gaz.

Lorsque les particules interagissent, il se produit d'importants champs de déformation d'athaction. Ces champs de déformation produisent une déformation plastique de nombreux métaux (macles), mais nous n'avons pas observé de macle dans l'aluminium ni dans le fer.

Zusammenfassung—Bildung, Wachstum und gegenseitige Wechselwirkung kleiner, durch Verdampfung im Gas erzeugter Metallpartikel wurde untersucht. Einzelne Metallatome diffundieren radial aus einer Verdampfungsquelle, bis sie bei einer Temperatur von etwa (0,35–0,40) T_m (T_m = absolute Schmelztemperatur) kondensieren. Die Partikel wachsen anschließend, überwiegend durch Zusammenlagern. Die Endgröße der Partikel ist bestimmt von Verdampfungstemperatur und Gasdruck.

Bei der Wechselwirkung zwischen Partikeln entstehen starke Adhäsions-Verzerrungsfelder. Diese Verzerrungen bedingen plastische Verformung (Zwillinge) in vielen Metallen; jedoch wurden keine Zwillinge beobachtet in Aluminium und in Eisen.

The interest in submicron metal particles has been growing during recent years. The reason for this interest stems partly from the many technological applications (smoke particles, welding fume, early stage sintering, etc.) and the investigations of fine powders have been facilitated by the gas evaporation method which is convenient for producing small particles of a desired size (which is increasing with gas pressure) and which have a quite narrow size distribution. A typical particle diameter when evaporating a metal in an inactive gas at a pressure of 10 torr is 40–60 nm. A considerable amount of work has been performed with this method mainly by Japanese workers, who have made a systematic examination of various metal particles [1–9]. They have primarily studied the particle size distribution and the particle shapes at various places around the evaporation source. Various models for particle growth have been suggested, mainly based on coalescence [10–14] and the models have been supported by measured particle distributions, but with few or no comments on the kinetics and the temperature.

We have in earlier investigations [15–19] made a detailed study of the various processes of adhesion between small single crystal particles and found that the adhesion process can be described as composed of several distinct steps. After the first contact between particles, adhesion causes an elastic and subsequently a plastic interaction between the particles. The surface energy supplies the driving force in these processes, which conveniently can be studied in the electron microscope. These phenomena are then, if the temperature is high enough, followed by sintering, which first of all will neutralize the strain fields at the contact. Further sintering will lead to a more continuous, necklace-like structure [18] and the final step is a complete sintering between the particles. Little was said however about the temperature at which the various processes occurred. It is the purpose of this paper to elucidate some aspects of particle formation and interaction with special emphasis on the temperature. One of the major problems in these temperature measurements is to take measurements in a system of small particles without disturbing the temperature distribution. Therefore the temperature should be determined using direct or indirect methods causing as small an interaction with the system as possible.

EXPERIMENTAL TECHNIQUE

The small metal particles used in this investigation (Ag, Al, Au, Co, Cr, Cu, Fe, Mg, Ni, Zn) were produced by evaporation from a conical tungsten basket in a pure argon atmosphere (99.9997%). The evaporation unit was pumped down to 2×10^{-5} torr, filled with argon gas to 300 torr, re-evacuated, and finally filled with argon mostly to a pressure of 10 torr. The particles were collected on carbon covered electron microscope grids at various places in the smoke cloud and subsequently observed in a JEM 200 A transmission electron microscope. Many of the particles were hanging freely from the microscope grids, but no difference was observed between these particles and those supported by the carbon film.

It was important during this investigation to determine the temperature with confidence at and around the evaporation source. The temperature of the evaporation source was determined with a pyrometer and the temperature in the gas was measured with fine thermocouples.

In order to detect the position of particle formation, photographs of the smoke cloud were taken. Another method of finding out where the various processes occurred was to arrange a chain of tungsten wire (diameter 0.5 mm) below, around and above the evaporation basket (Fig. 1). Different types of condensates are developed at various places in the smoke and these were subsequently observed in a JSMU-3 scanning electron microscope. There is, of course, a heat conduction in the wires, which will slightly deform the temperature distribution, but this has been reduced to a large extent by using fine wire and a chain structure. One has also to take into account a possible sintering effect for the condensates as they are at the recorded temperature for a longer time than the ordinary particles. We do not consider this effect important, however, as the outer surface layer, which formed just before switching off the power, should give quite a true picture of the process.

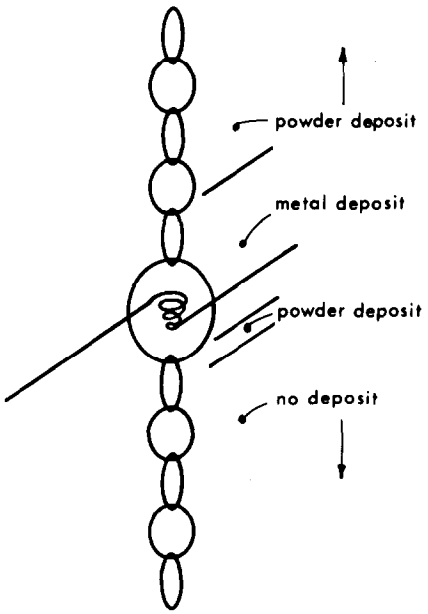

Fig. 1. Chain of tungsten wires mounted around the evaporation source. Closest to the source a metal film is found on the wire and further out powder. No deposit is detected below 10–15 mm underneath the source.

The temperature measurements as described above were performed during gold evaporation, although the same type of smoke cloud and general behaviour was observed for all the metals, at least when the gas pressure was 10 torr or above.

A totally different method of gaining temperature information was obtained by using ferromagnetic material. The Curie temperature for such particles is an excellent temperature probe. These particles eventually form a string-like structure, which means that final agglomeration has occurred below the Curie temperature.

EXPERIMENTAL RESULTS

Smoke characteristics and temperature measurements

The smoke cloud from the evaporation source has a very characteristic shape as seen in Fig. 2. The smoke cloud, which in this case is produced at a pressure of 20 torr is not, however, as pronounced when viewed at a lower pressure as has also been reported [4, 6, 7]. The bottom part of the cloud is, to a good approximation, a half sphere, while the smoke zone above the source has a cylindrical shape until it hits the walls of the evaporation unit, where it is deflected. The radius of the cylinder decreases with distance from the source (and with temperature) until it becomes more or less constant. Figure 2 also clearly shows that the boundaries look denser than the interior of the smoke cloud. If the density of smoke particles were constant throughout the cloud, the interior would appear much denser than the edges. This strongly suggests that the smoke particles are mainly found along *the walls* in a shell or tubelike structure and few light scattering particles are thus seen in the smoke interior. This is substantiated by other investigations [4, 7], where it is found that the number of particles collected above the source in the interior zone (and in the outer zone) is not as large as the number of particles found along the rim of the smoke cloud.

During evaporation, a vertical convection current is set up in the argon gas. The velocity of this convection current is estimated to be 0.1–1 m s^{-1}. The few particles collected in the interior of the tube are generally much more facetted than the bulk of particles, which might be due to the smaller contact with the surrounding and relatively more impure argon gas. This facetted shape does on the other hand also indicate a complete sintering process between originally smaller particles [18]. In a continuing sintering process the shapes are markedly rounder.

The temperature in the smoke zone as determined with thermocouples for various gas pressures is seen

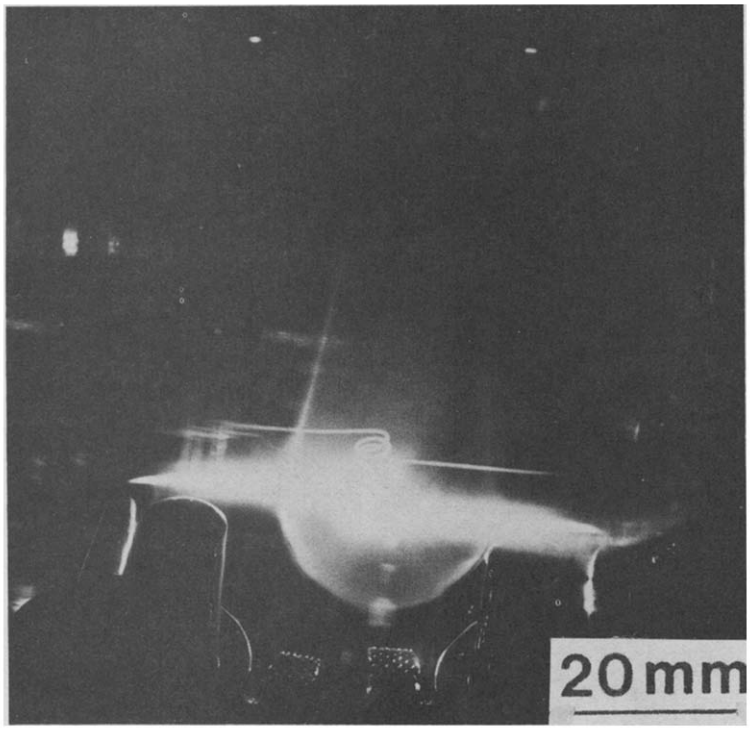

Fig. 2. Smoke cloud of gold particles. Evaporation pressure 20 torr.

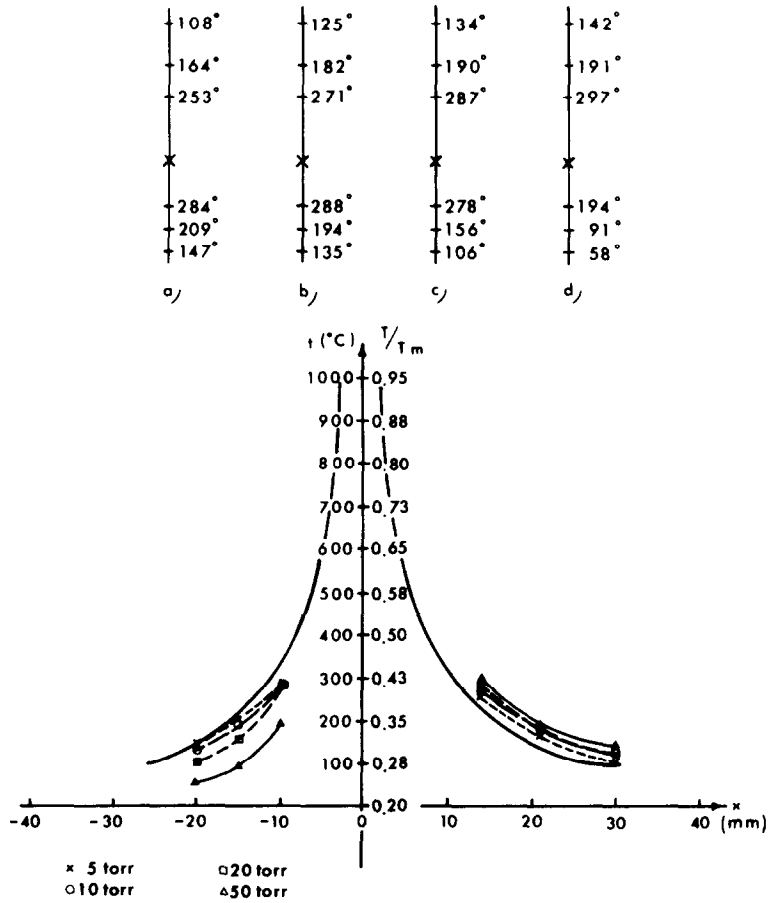

Fig. 3. Measured temperature around the evaporation source at various pressures. The source temperature is 1500°C. (a) $p = 5$ torr; (b) $p = 10$ torr; (c) $p = 20$ torr; (d) $p = 50$ torr; (e) measured temperature profiles at the various pressures. The fully drawn curve is calculated under the assumption of radiation equilibrium between the particles and the source and shows roughly an inverse square dependence. No consideration is then taken to the heat transport through convection.

in Fig. 3. It should be noted that the temperature in the lower part of the smoke cloud is roughly 0.35–0.40 T_m, where T_m is the absolute melting temperature for gold particles. This can be inferred from a comparison with the smoke cloud in Fig. 2 and Fig. 3. The radius of the smoke cloud varies from 8–9 mm at 50 torr to roughly 15 mm at 10 torr. The appearance of the thin wires running across the smoke zone strongly suggests that the lower half part of the smoke cloud is the main formation zone for particles. The wires closest to the evaporation source were covered with gold [Fig. 4(a)]. Further out there was a brown

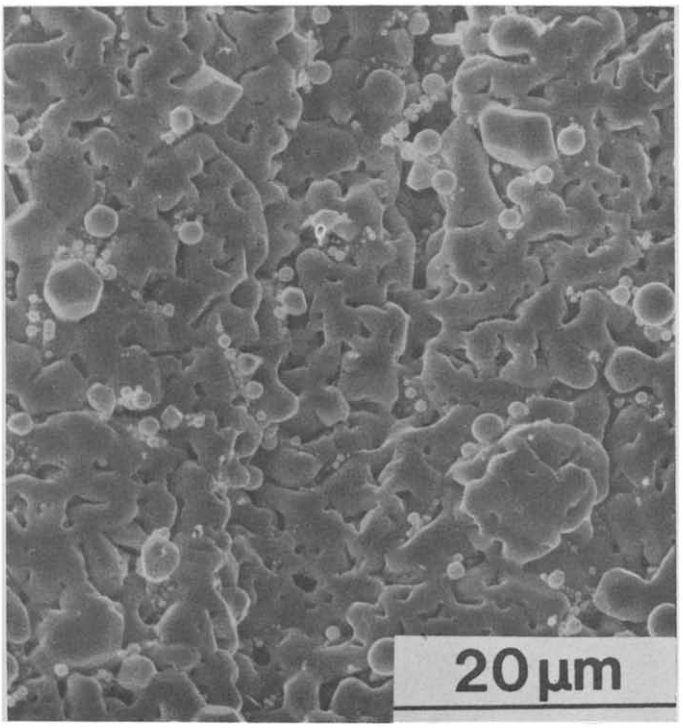

Fig. 4(a).

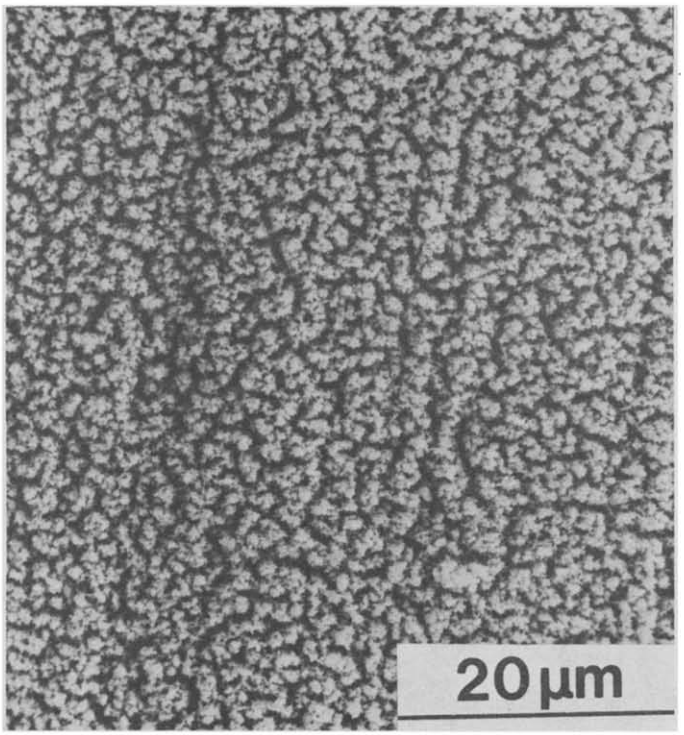

Fig. 4(b).

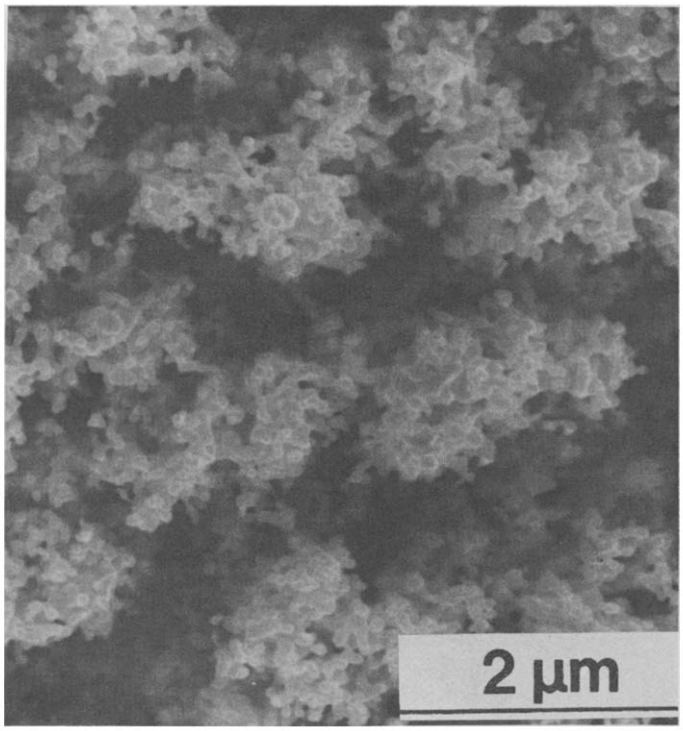

Fig. 4(c).

Fig. 4. Various deposits of gold collected on the wire structure. (a) Deposit in the metal region; (b) Deposit in the powder region; (c) Same as (b). Higher magnification.

reddish powder covering the wires and still further up a denser and darker region of the same powder was found. Somewhat below the source (10–15 mm) depending on pressure and further down no traces of material were observed. Smoke particles collected in the 'brown-reddish' area are shown in Fig. 4(b) and (c), where the peculiar island pattern from Fig. 4(a) is repeated. Figure 4(a) could have evolved from a structure similar to Fig. 4(b) and (c) by sintering. The observed pattern is also known from evaporation studies of gold on glass substrates and is assumed to be due to electrostatic forces [20].

As in other investigations it was found here that the particle size distribution was log–normal and that the average particle size increases with gas pressure [3, 4, 12]. The average evaporation rate was measured at 1500°C by noting the complete evaporation time for a known amount of material and for gold this was found to be 3.8×10^{18} atom s^{-1}.

In order to get a further insight into the process, some ferromagnetic (Co, Fe, Ni) materials were evaporated and the magnetic properties of these materials were used as a temperature probe. The particles of these materials form long singlelined chains as has been reported earlier [8, 19], and this is an indication of the temperature at which final agglomeration of particles occurred (Fig. 5). The magnetic data for these materials are given in Table 1 and one should here only note the variation in Curie temperature of the different materials and that the stable structure for small particles of cobalt is f.c.c.

Metallography of particles

Particles of the various metals exhibit the same characteristic features as has been reported in detail earlier for gold particles. First of all, the particles often have a pronounced facetted shape with mainly low-indexed crystallographic planes as boundaries and often with slightly rounded corners and edges. Secondly, the particles form long chains with many branches (the branches are more or less absent in the ferromagnetic materials) and with very minute contact zones between the particles, often along low indexed planes. In some cases strain fields were observed in the as-produced particles (Fig. 6). In the earlier reported work on gold particles this was not detected in the newly formed particles, but only when the particles were ripped apart at room temperature and then allowed to react again. In the present investigation adhesion strain fields were seen in silver, magnesium (very pronounced effect) and nickel in the freshly produced particles but it was far from observed at all contacts. As the strain fields are visible in the nickel particles, one is sure that the formation of that contact has occurred below the Curie temperature ($0.38\ T_m$) in this material, and that the magnetic transformation has caused a rearrangement of particles.

The only defects seen in the particles were twins and they were observed abundantly in a number of different materials, namely gold, silver, copper, nickel (Fig. 6, 7), magnesium (Fig. 6) and zink (Fig. 8). No

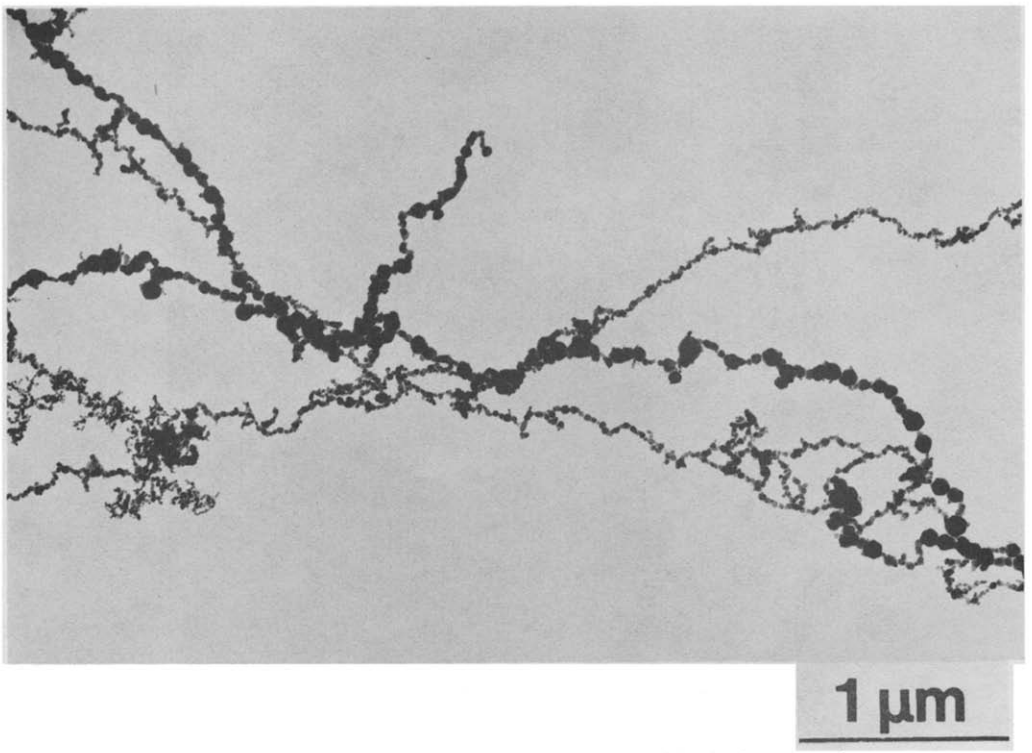

Fig. 5. Strings of cobalt particles. Note the constant particle size in each string.

Table 1.

Material of particles	Crystal structure	Curie temp, T_c (K)	Melt temp, T_m (K)	T_c/T_m	Satur. magn. field (Vs m^{-2})
Co	f.c.c.	1400	1765	0.81	1.82
Fe	b.c.c.	1043	1803	0.61	2.19
Ni	f.c.c.	631	1725	0.38	0.64

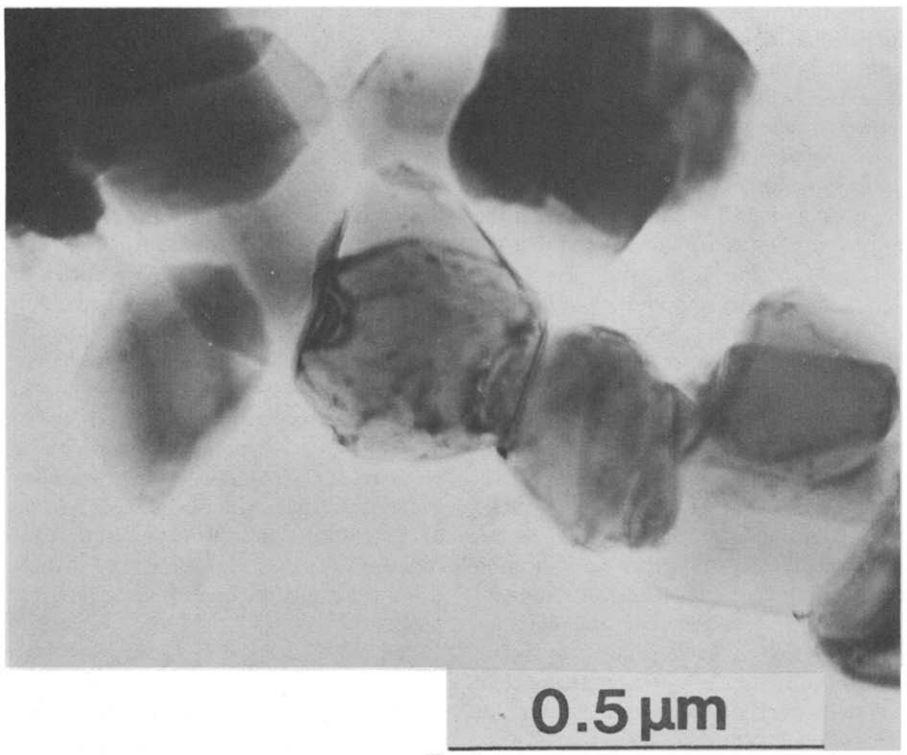

Fig. 6(a).

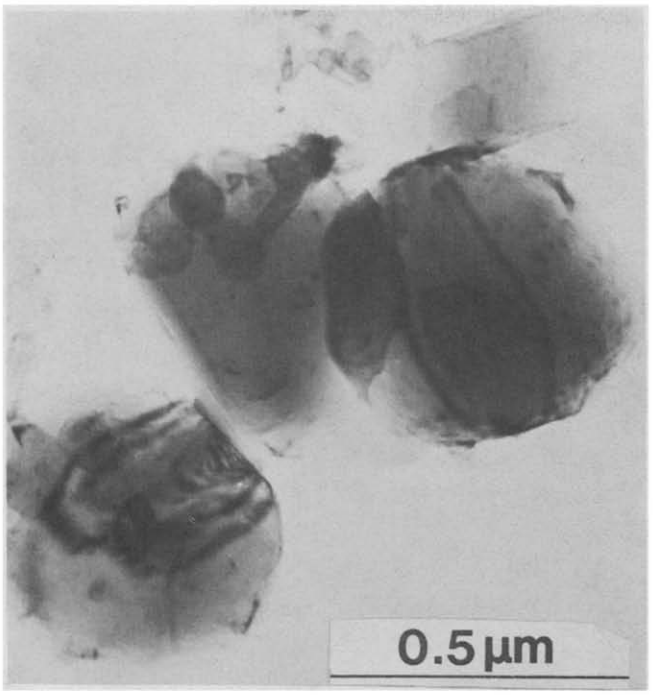

Fig. 6(b).

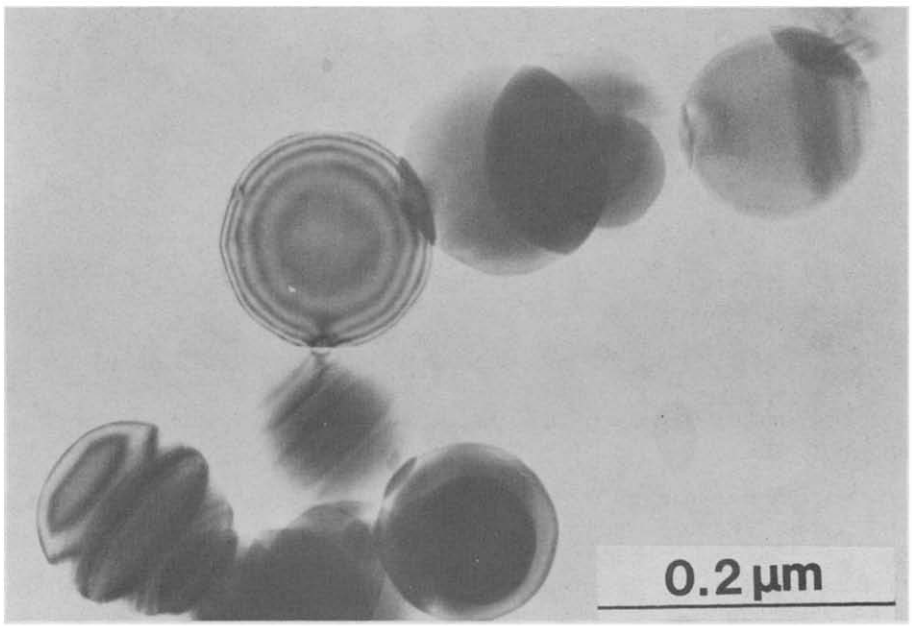

Fig. 6(c).

Fig. 6. Adhesion strain fields (a, b) Magnesium particles. Note twins associated with contacts; (c) nickel particles.

twins were observed in iron and aluminium, where the stacking fault energy and twin energy is high. In the absolute majority of cases, the twins were associated with the contact zone (Fig. 6, 7), which was first reported for gold particles [16–18], but this also holds true for all other materials. It should be mentioned here that twin formation during coalescence has also been observed during vacuum deposition of gold onto molybdenum disulphide [21].

The same deformation pattern which was observed for the gold crystals, was also found for other materials. According to the picture from the gold work, the original adhesion between the particles causes such high stresses along the periphery of the adhesion circle that plastic deformation can be launched in the surrounding material. As the slip geometry is the same in the f.c.c. materials, very similar patterns evolve in these cases.

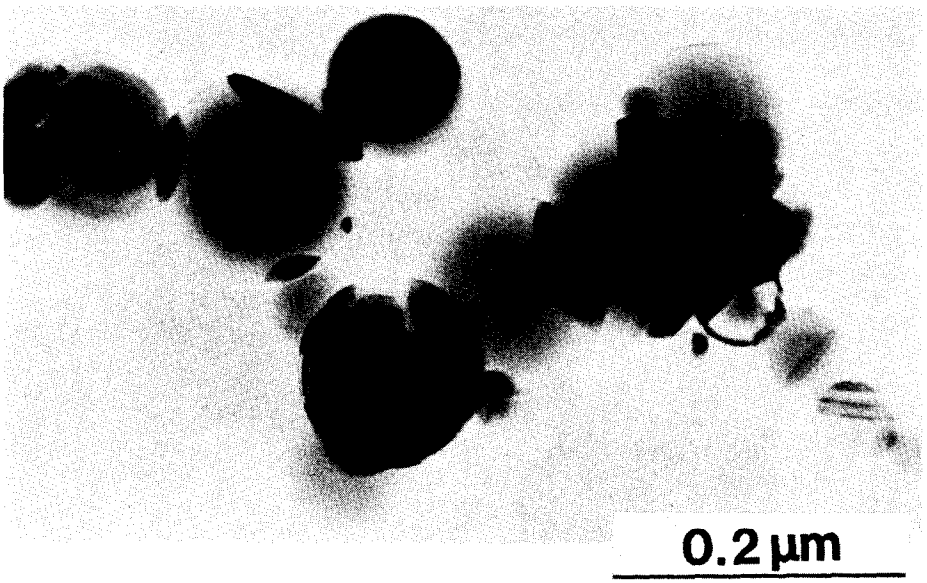

Fig. 7. Nickel particles. A twin is created at the particle–particle contact due to the adhesion strain field.

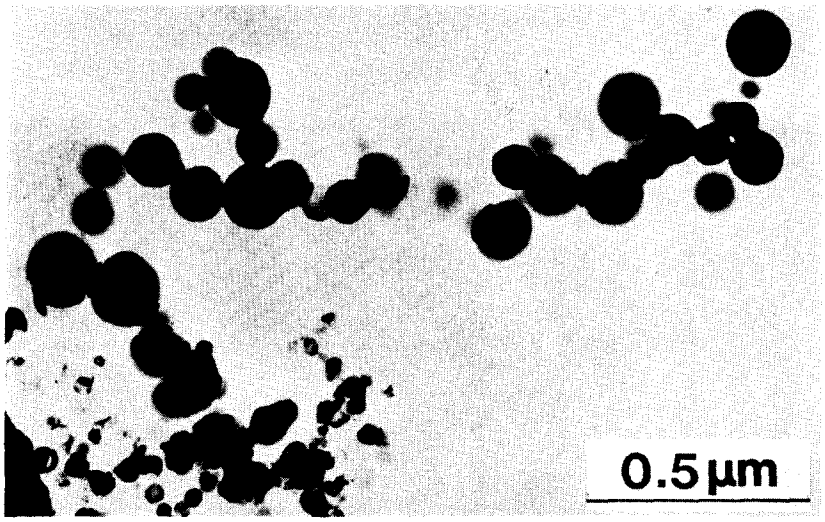

Fig. 8. Zinc particles. Note twinning in many particles. Most of the black contrast is however due to an effect of overlapping particles.

No dislocations were ever found in the particles, which certainly is due to the proximity to the surfaces, and the only other defect visible, besides the twins, was a very fine faulting in the cobalt particles (Fig. 9), which might be fine twins or stacking faults. The structure of such small cobalt particles is f.c.c. although the bulk structure is h.c.p. The stacking fault energy and the twin energy should be quite low in this case.

The particles of the magnetic materials exhibit a peculiar pattern. The particles belonging to one string have almost identical sizes, while particles from another chain collected during the same evaporation might be different, but still of constant particle size (Fig. 5). This shows the importance of 'particle history'. The different sizes indicate that the particles have formed in various parts and followed different trajectories before final collection.

In some places very small particles of similar size were found in dense networks (Fig. 10). Even in such small particles, twins were observed down to a particle diameter of around 10 nm. These clusters of particles might be considered as a 'frozen in' part of the early particle history. If this is the case it illustrates the importance of diffusion and diffusion lengths in particle growth. Twinning in small particles has also been treated in [22], where it was reported that multiple twinning occurs spontaneously to lower surface energy.

DISCUSSION

Diffusion in the gas

It is obvious that metal atoms leave the evaporation source in all directions; pure gold is found on the whole wire structure in the vicinity of and sur-

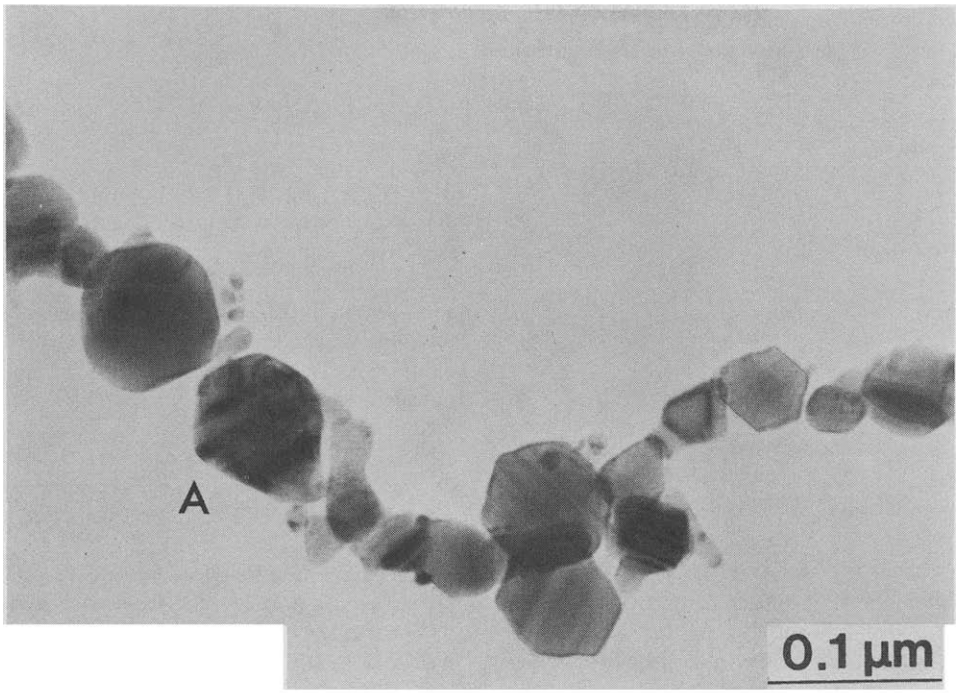

Fig. 9. Cobalt particles with many twins. In the particle marked A, there is also a fine twinning or fine stacking faults on a second plane.

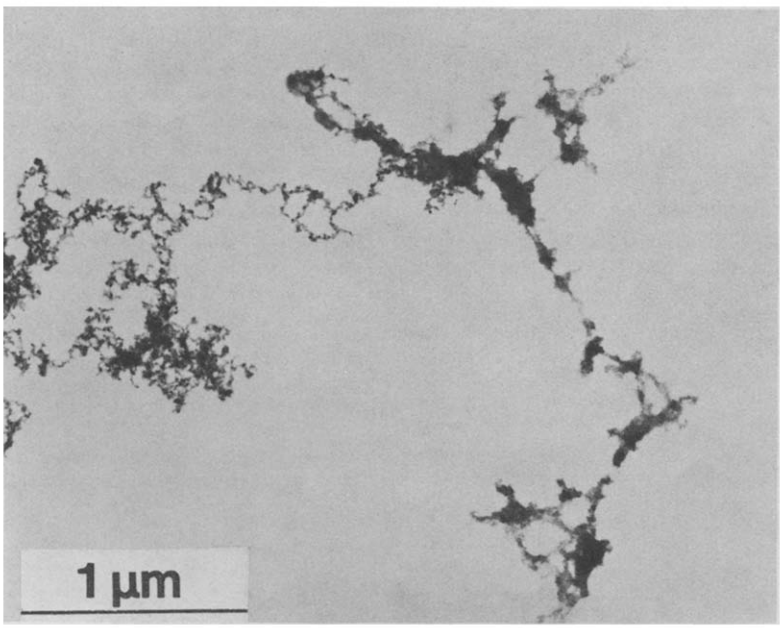

Fig. 10. Iron particles. In one half of the picture the particles have one size, and in the other half also a constant but smaller size.

rounding the source. It is also very obvious that the particles, once formed, have such low drift velocity that the convection in the argon gas totally governs the particle trajectories. We will now try to get a more complete picture of the material transport through the gas.

When single metal atoms are ejected out into the gas from the evaporation source, they must diffuse through the gas. It is quite easy to find the effective diffusion (drift) velocity for single atoms or particles and then compare this result with the convection current in the gas. The drift velocity decreases outwards and when it becomes comparable in size with the convection current (but with opposite sign) somewhere below the source, the atoms (particles) can make no further progress downwards. One has then, in fact, found the lower boundary of the smoke shell.

If we consider a radial diffusion out from a spheri-

cal source into a medium which is at rest (neglecting for a moment the gas convection), the relations below are obeyed.

$$j = -D\frac{\partial n}{\partial r},$$

$$n = \frac{C_1}{4\pi D r},$$

$$j = \frac{C_1}{4\pi r^2}.$$

But

$$j = n \cdot v_{\text{drift}}$$

$$\Rightarrow v_{\text{drift}} = \frac{j}{n} = \frac{D}{r},$$

where

j = number of diffusing atoms (particles)/unit area, time (m^{-2} s),
n = number of diffusing atoms (particles)/unit volume (m^{-3}),
v_{drift} = drift velocity outwards of metal atoms (particles) (m s^{-1}),
C_1 = number of evaporated atoms/unit time (s^{-1}),
r = distance from centre of source (m),
R = particle radius (m),
ρ = density of material (kg m^{-3}),
n_0 = number of argon atoms/unit volume (m^{-3}),
T = absolute temperature (K),
M = molecular weight (kg $kmol^{-1}$),
D = diffusion coefficient (m^2 s^{-1}),

$$D = \sqrt{\frac{N_0 kT}{6\pi^2 M}} \cdot \frac{1}{(R_{\text{Me}} + R_{\text{Ar}})^2} \cdot \frac{1}{n_0}$$

for atomic diffusion,

$$D = \sqrt{\frac{kT}{8\pi^3 \rho R^7}} \frac{1}{n_0}$$ for particle diffusion,

N_0 = Avogadro's number (atoms $kmol^{-1}$),
R_{Me} = radius of metal atoms (m),
R_{Ar} = radius of argon atoms (m).

The expressions above are derived assuming constant diffusion coefficient, D, and constant temperature. If these expressions are now used with a varying diffusion coefficient, the drift velocity for metal atoms outside a source can be found for various temperatures and is shown in Tables 2, 3 for a specific r, 10 mm. In reality, D is decreasing outwards as T is decreasing and n_0 is increasing. The decrease in n_0 is noted as the swelling of the smoke cloud near the source.

When the diffusion coefficient thus gets smaller further out, it is in fact the lower D that will determine the rate of diffusion in a given case. Thus it is justified to use a constant D at the points of interest (particle formation).

It is seen that v_{drift} varies both with gas pressure and temperature. If the gas pressure is doubled and the evaporation temperature is kept constant, the convection current decreases to half its original value to a first approximation. (The gas has now a higher capacity for the necessary heat transport, which is determined only by the source temperature.) But at the same time, the diffusion coefficient and the drift velocity also decrease to half their original values (if the temperature is constant). If the competition between outgoing drift velocity and convection current is governing the process, then this competition

Table 2. The diffusion coefficient of the gold atoms in argon gas at various pressures and temperatures $v_{\text{drift}} = D/r$

T/T_m	t (°C)	p = 5 torr D (m^2 s^{-1})	p = 10 torr D (m^2 s^{-1})	p = 20 torr D (m^2 s^{-1})
0.05	−206	0.11×10^{-3}	0.57×10^{-4}	0.28×10^{-4}
0.10	−139	0.32×10^{-3}	0.16×10^{-3}	0.80×10^{-4}
0.15	−73	0.59×10^{-3}	0.30×10^{-3}	0.15×10^{-3}
0.20	−6	0.91×10^{-3}	0.45×10^{-3}	0.23×10^{-3}
0.25	61	0.13×10^{-2}	0.63×10^{-3}	0.32×10^{-3}
0.30	128	0.17×10^{-2}	0.83×10^{-3}	0.42×10^{-3}
0.35	195	0.21×10^{-2}	0.11×10^{-2}	0.53×10^{-3}
0.40	261	0.26×10^{-2}	0.13×10^{-2}	0.64×10^{-3}
0.45	328	0.31×10^{-2}	0.15×10^{-2}	0.77×10^{-3}
0.50	395	0.36×10^{-2}	0.18×10^{-2}	0.90×10^{-3}
0.55	462	0.41×10^{-2}	0.21×10^{-2}	0.10×10^{-2}
0.60	529	0.47×10^{-2}	0.24×10^{-2}	0.12×10^{-2}
0.65	595	0.53×10^{-2}	0.27×10^{-2}	0.13×10^{-2}
0.70	662	0.60×10^{-2}	0.30×10^{-2}	0.15×10^{-2}
0.75	729	0.66×10^{-2}	0.33×10^{-2}	0.17×10^{-2}
0.80	796	0.73×10^{-2}	0.36×10^{-2}	0.18×10^{-2}
0.85	863	0.80×10^{-2}	0.40×10^{-2}	0.20×10^{-2}
0.90	929	0.87×10^{-2}	0.43×10^{-2}	0.22×10^{-2}
0.95	996	0.94×10^{-2}	0.47×10^{-2}	0.24×10^{-2}
1.00	1063	0.10×10^{-1}	0.51×10^{-2}	0.25×10^{-2}

Table 3. Thermodynamical calculation of metal particle nucleation in argon gas of different pressures

Substance	T/T_m	r_{crit} (nm)	ΔF (ev)	$p = 5$ torr v_D ($m\,s^{-1}$)	$p = 5$ torr n_n (m^{-3})	$p = 10$ torr v_D (m^{-1})	$p = 10$ torr n_n (m^{-3})	$p = 20$ torr v_D ($m\,s^{-1}$)	$p = 20$ torr n_n (m^{-3})
Au	0.35	0.10	0.35	0.21	0.26×10^{19}	0.11	0.53×10^{19}	0.053	0.11×10^{20}
Ag	0.30	0.11	0.41	0.20	0.20×10^{18}	0.10	0.39×10^{19}	0.050	0.79×10^{18}
Al	0.45	0.09	0.23	0.49	0.12×10^{20}	0.24	0.24×10^{20}	0.12	0.47×10^{20}
Co	0.30	0.10	0.58	0.53	0.16×10^{17}	0.27	0.33×10^{17}	0.13	0.65×10^{17}
Cr	0.25	0.11	0.67	0.58	0.36×10^{16}	0.29	0.71×10^{16}	0.14	0.14×10^{17}
Cu	0.35	0.09	0.37	0.43	0.78×10^{18}	0.21	0.16×10^{19}	0.11	0.31×10^{19}
Fe	0.30	0.11	0.70	0.56	0.16×10^{16}	0.28	0.32×10^{16}	0.14	0.64×10^{16}
Mg	0.25	0.20	0.69	0.19	0.15×10^{8}	0.094	0.30×10^{8}	0.047	0.59×10^{8}
Mo	0.30	0.11	0.72	0.79	0.25×10^{18}	0.40	0.51×10^{18}	0.20	0.10×10^{19}
Ni	0.30	0.09	0.45	0.52	0.25×10^{18}	0.26	0.49×10^{18}	0.13	0.99×10^{18}
Pb	0.50	0.15	0.31	0.087	0.19×10^{18}	0.043	0.38×10^{18}	0.022	0.75×10^{18}
Pt	0.35	0.10	0.63	0.42	0.27×10^{18}	0.21	0.55×10^{18}	0.10	0.11×10^{19}
Sn	0.75	0.10	0.17	0.19	0.12×10^{21}	0.097	0.25×10^{21}	0.044	0.49×10^{21}
W	0.25	0.08	0.51	0.61	0.78×10^{19}	0.30	0.16×10^{20}	0.15	0.31×10^{20}
Zn	0.30	0.19	0.83	0.11	0.18×10^{3}	0.057	0.36×10^{3}	0.028	0.72×10^{3}
Evaporation pressure 0.01 torr									
Au	0.40	0.10	0.36	0.26	0.48×10^{19}	0.13	0.97×10^{19}	0.064	0.19×10^{20}
Ag	0.35	0.12	0.38	0.25	0.46×10^{18}	0.13	0.93×10^{18}	0.063	0.19×10^{19}
Al	0.45	0.09	0.21	0.49	0.18×10^{20}	0.24	0.36×10^{20}	0.12	0.72×10^{20}
Co	0.35	0.10	0.62	0.67	0.39×10^{17}	0.34	0.77×10^{17}	0.17	0.15×10^{18}
Cr	0.25	0.11	0.62	0.58	0.11×10^{17}	0.29	0.21×10^{17}	0.14	0.42×10^{17}
Cu	0.35	0.09	0.35	0.43	0.15×10^{19}	0.21	0.30×10^{19}	0.11	0.61×10^{19}
Fe	0.30	0.11	0.65	0.56	0.48×10^{16}	0.28	0.95×10^{16}	0.14	0.19×10^{17}
Mg	0.25	0.19	0.63	0.19	0.27×10^{9}	0.094	0.54×10^{9}	0.047	0.11×10^{10}
Mo	0.30	0.10	0.67	0.79	0.50×10^{18}	0.40	0.99×10^{18}	0.20	0.20×10^{19}
Ni	0.35	0.09	0.48	0.66	0.48×10^{18}	0.33	0.95×10^{18}	0.16	0.19×10^{19}
Pb	0.55	0.15	0.31	0.10	0.53×10^{18}	0.050	0.11×10^{19}	0.025	0.21×10^{19}
Pt	0.35	0.10	0.59	0.42	0.54×10^{18}	0.21	0.11×10^{19}	0.10	0.22×10^{19}
Sn	0.85	0.10	0.16	0.21	0.17×10^{21}	0.097	0.34×10^{21}	0.053	0.69×10^{21}
W	0.30	0.09	0.55	0.80	0.12×10^{20}	0.40	0.23×10^{20}	0.20	0.46×10^{20}
Zn	0.30	0.18	0.76	0.11	0.97×10^{4}	0.057	0.19×10^{5}	0.028	0.38×10^{5}
Evaporation pressure 0.1 torr									

The results are given for that temperature, where the maximum density of nuclei is obtained. r_{crit} = critical radius at nucleation. F = critical energy. $v_D = D/r$ = drift velocity. n_n = density of nuclei.
N.B. Mg and Zn smoke forms by sublimation.

should yield densification in roughly the same place. This is not totally so, as the temperature distribution around the source depends on the gas pressure (Fig. 3) and we shall find that the temperature plays a crucial role. The fact remains, however, that the smoke shell always ends about 10–15 mm below the source.

Streamlines in the gas

One remarkable property of the particle cloud is its lower half spherical shape. A complete description of the atom (particle) trajectories and thereby the shape of the cloud would in principle be tractable knowing the complete temperature and pressure distribution. We shall here simply assume that the transport occurs by single atoms diffusing radially outwards and that this movement is superposed on a constant vertical convection current, v_c. As is shown earlier, the lowest part of the shell would then be $r = D/v_C$ below the source. The complete streamline pattern is shown in Fig. 11, where also the envelope outside which no atoms can reach, is drawn. This pattern resembles the observations (Fig. 2) but with at least one difference, which is that the real smoke tube gets narrower above the source. This phenomena is, however, partly a temperature effect. In reality the gas inside the shell gets cooler as it rises above the source and therefore the tube shrinks in diameter and this fact is not considered in Fig. 11. From the experiments it is found that the temperature out from the source decreases roughly with the inverse square of radius (Fig. 3) and this can easily be fitted with a picture where the temperature is governed by radiation.

Another difference between theory and experiment is the actual bottom shape of the cloud. The streamline pattern with all its assumptions does not predict a half spherical boundary, although there is a similarity. The spherical shape is probably a temperature effect and it will be dealt with in the next paragraph.

Formation zone for particles

The important remaining factors to deal with are the formation and further growth of particles. As most particles are seen in the shell, it is reasonable to believe that the majority of nucleation takes place there. When metal atoms have diffused outwards and

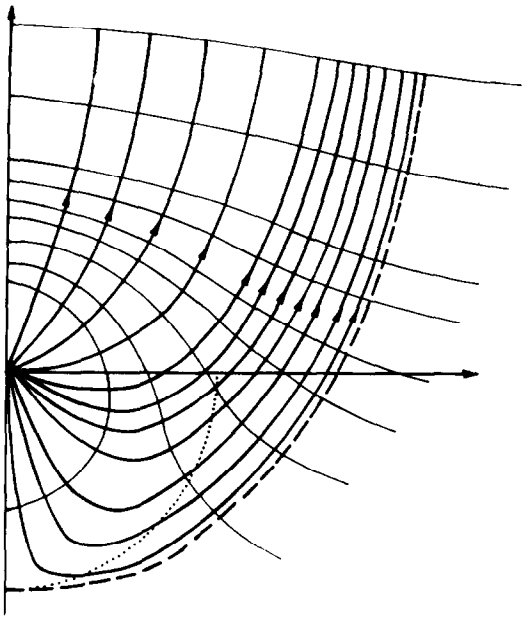

Fig. 11. Streamline pattern. This figure shows a superposition of radial atomic diffusion out from a source and a vertical convection current.

encountered the convection current, there must be a densification of material (metal atoms) and probably a particle formation. Once formed, these particles, however, cannot continue to move along the streamlines in Fig. 11 as the diffusion drift velocity falls very rapidly indeed as the radius of particles increases (see above). These particles would then move more or less vertically upwards (but with a slight curvature, due to variation in n_0) and the smoke cloud would look much denser internally. The reason for the small number of particles in the interior is probably due to a re-evaporation of particles as they re-enter into the region with higher temperature. Once re-evaporated, the atoms start diffusing outwards again until new particles are formed at the temperature wall. Most particles would then 'bounce' on the temperature wall until they have roughly reached the level of the source after which they are free to move upwards. A sketch of the proposed process is shown in Fig. 12. The temperature profile from the source is almost spherical close to the source, but obviously becomes more and more distorted further out from the source. This fact, in connection with the spherical form of the lower part of the smoke cloud, strongly suggests that temperature is the governing factor in particle formation and that the atoms do not really reach as far out as would be predicted by $r = D_{atom}/v_c$. In the case of gold, all the experiments show that the critical temperature is roughly 0.35–0.40 T_m.

Nucleation and growth of particles

It is possible to apply a classical thermodynamic calculation on particle nucleation and thus predict where it should occur. To simplify, we again assume pure diffusion out from the source and ignore the convection current for a moment. The diffusion coefficient is also assumed to be independent of temperature. Under these circumstances, the density of gold (metal) atoms diffusing out from the gas is given by the expression

$$n = \frac{C_1}{4\pi D r}.$$

The equilibrium vapour pressures for pure metals are found in (23–25) as a function of temperature.

On the other hand the equilibrium vapour pressure above a spherical surface is higher by a factor

$$\frac{p}{p_0} = \exp(2M\sigma/rRT\rho),$$

M = molecular weight (kg kmol^{-1}),
σ = surface energy (Jm^{-2}),
R = gas constant (Nmkmol^{-1} K^{-1}),
T = absolute temperature (K),
r = particle radius (m),
n = number of metal atoms/unit volume (m^{-3}),
ρ = density of particles (kg m^{-3}),
p = vapour pressure (Nm^{-2}),
p_0 = equilibrium vapour pressure (Nm^{-2}).

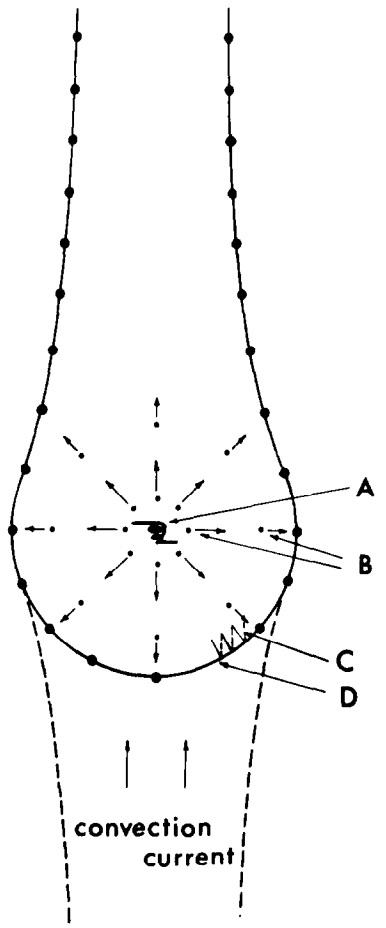

Fig. 12. The various steps in particle formation. A. Evaporation source, B. Atoms diffusing outwards, C. A possible sequence of particle formation, re-evaporation, particle formation etc. The diffusion velocity for particles is significantly lower than for atoms, D. Boundary of the smoke cloud.

This leads to the well known expression for the nucleation radius

$$r_{\text{nucl}} = \frac{2M\sigma}{RT\rho \ln p/p_0}.$$

The critical energy for nucleation

$$\Delta F = \frac{4\pi}{3}\sigma r_{\text{nucl}}^2.$$

The density of nuclei/unit volume $= n_n(\text{m}^{-3})$

$$n_n = n \exp\{-\Delta F/kT\}.$$

Such calculations were performed for various metals assuming critical evaporation pressures of 0.01 mm Hg and 0.1 mm Hg respectively (7). The maximum density of nuclei and other relevant data are shown in Table 3.

The distance from the source is assumed to be 10 mm in all these calculations, but results for other distances can easily be found by scaling.

From this table it can be inferred that classical thermodynamics alone cannot explain the results. Neglecting such problems as the influence of convection current and also the strong influence of temperature on the diffusion coefficient it is obvious that the critical nucleation radii are too small and not within reach for classical thermodynamics, as one is down on atomic dimensions.

Nevertheless, the temperature at maximum nucleation probability seems to fall in the correct range (0.30–0.45 T_m for most metals) compared to the experimentally found results. Additionally, the diffusion drift velocity at the actual temperature seems to be of the same order of magnitude as the estimated convection current. When particles form, the diffusion velocity goes down with R^{-7} (R = particle radius) and thereby diminishes drastically.

The results from the last paragraph are thus further supported, but one important question remains, and that is how the particles grow.

This problem is approached indirectly. Assume first that small particles have formed in the outer shell. Depending on the convection current, these particles will be at the nucleation temperature roughly for a period of

$$\frac{\pi r}{2v_{\text{conv}}} = \frac{\pi r^2}{2D} = \frac{\pi(14 \times 10^{-3})^2}{2 \times 0.11 \times 10^{-2}} = 0.28 \text{ s}.$$

(These figures are for gold particles 10 torr and with a gas shell radius of 14 mm.)

If we now look at sintering rates for small gold particles, we find that 0.35 s is the coalescence (complete sintering) time for particles of radius 10 nm at 200°C, 20 nm at 300°C, 30 nm at 400°C respectively. These results are from (26). These radii are only slightly lower than the ones obtained at $T/T_m = 0.35$ and this lends strong support to a coalescence mechanism. The coalescence time is proportional to the fourth power of the radius and to the diffusion coefficient of the metal. If we assume that the sintering speed governs the final radius of the particles and that this radius is 20 nm, then particles one tenth of that size should sinter 10^4 faster than the time for the whole passage and that means immediately. Thus coalescence in the beginning is very rapid and the last steps will govern the process. The question of whether growth of particles to an important extent also occurs by absorption of single atoms cannot completely be answered, but the results of [10–12] are certainly also in favour of a coalescence type of growth.

One further piece of evidence to support the picture above can be obtained from the particle mean size at various pressures. When the pressure increases, the convection current goes down and the particles are at temperature for a longer time. For example, if the pressure is doubled, particles of size $R^4\sqrt{2}$ should be found instead of particles with radius R. This result fits quite well with the experiments.

Provided that the pressure is kept constant, it is found that the mean size of particles increases with atomic weight of the inert gas used during evaporation [7]. A higher atomic weight of the inert gas will lead to a lower convection current and thus the particles will be at temperature for a longer time, resulting in larger particles.

When the temperature of the evaporation source is increased, the particle size also increases [3–4]. This result is supported by the results in Table 3, where it is clearly seen that there is a tendency for particle formation at higher temperatures, when the evaporation pressure (temperature) increases. If this is correct, the particle coalescence after nucleation is determined by the higher temperature and this will lead to a larger particle size.

CONCLUSIONS

1. When a metal is evaporated in a gas of low pressure, the metal atoms diffuse radially outwards. At the same time a convection current is set up and the actual trajectories of metal atoms will be a superposition of these two movements.

2. When the metal atoms enter a colder region, particles are nucleated. This happens at a temperature of roughly 0.35–0.40 T_m.

3. The diffusion velocity of particles is much lower than for single atoms, and the particle trajectories are therefore only determined by the convection current.

4. When particles re-enter into the hot zone, they are very likely to reevaporate, as few particles are found there.

5. The particles mainly grow by coalescence. Larger particles are formed when the evaporation temperature or the gas pressure is higher.

6. Adhesion strain field fringes were seen in some of the as-produced particles (Ag, Mg and Ni). This suggests that the final contact between the particles has occurred at a lower temperature than 0.30–0.35 T_m, as otherwise, the elastic strain field at the contact, would have been reduced by partial sintering.

7. Plastic deformation (twins) were observed in Au, Ag, Co, Cu, Mg, Ni, Zn. No twins were seen in Al and Fe. Dislocations were never detected.

REFERENCES

1. K. Kimoto, Y. Kamiya, M. Nonoyama and R. Uyeda, *Jap. J. appl. Phys.* **2,** 702 (1963).
2. K. Kimoto and I. Nishida, *Jap. J. appl. Phys.* **6,** 1047 (1967).
3. S. Yatsuya, R. Uyeda and Y. Fukano, *Jap. J. appl. Phys.* **11,** 408 (1972).
4. S. Yatsuya, S. Kasukatse and R. Uyeda, *Jap. J. appl. Phys.* **12,** 1675 (1973).
5. S. Kasukabe, S. Yatsuya and R. Uyeda, *Jap. J. appl. Phys.* **13,** 1714 (1974).
6. I. Nishida and K. Kimoto, *Jap. J. appl. Phys.* **14,** 1425 (1975).
7. T. Ohno, S. Yatsuya and R. Uyeda, *Jap. J. appl. Phys.* **15,** 1213 (1976).
8. T. Hayashi, T. Ohno, S. Yatsuya and R. Uyeda, *Jap. J. appl. Phys.* **16,** 705 (1977).
9. Y. Saito, S. Yatsuya, K. Mikama and R. Uyeda, *Jap. J. appl. Phys.* **17,** 291 (1978).
10. L. Fritsche, F. Wolf and A. Schaber, *Z. Naturf.* **16a,** 31 (1961).
11. Y. Mizushima, *Z. Naturf.* **16a,** 1260 (1961).
12. C. G. Granqvist and R. A. Buhrmann, *J. appl. Phys.* **47,** 2200 (1976).
13. C. Kaito, K. Fujita and H. Shibahara, *Jap. J. appl. Phys.* **16,** 697 (1977).
14. C. Kaito, *Jap. J. appl. Phys.* **17,** 601 (1978).
15. K. E. Easterling and A. R. Thölén, *Acta metall.* **20,** 1001 (1972).
16. I. Hansson and A. Thölén, *Scand. J. Metall.* **6,** 27 (1977).
17. I. Hansson and A. Thölén, *Scand. J. Metall.* **7,** 33 (1978).
18. I. Hansson and A. Thölén, *Phil. Mag.* **37,** 535 (1978).
19. I. Hansson and A. Thölén, *Ninth International Congress on Electron Microscopy, Toronto* 1978, Vol. I, p. 582 (1978).
20. T. Andersson, Electrical and structural properties of ultrathin gold films on glass, Ph.D. Thesis, Chalmers Univ. of Technology, Gothenburg (1976).
21. M. H. Jacobs, D. W. Pashley and M. J. Stowell, *Phil Mag.* **13,** 129 (1966).
22. M. Gillet, *Surface Sci.* **67,** 139 (1977).
23. *Handbook of Chemistry and Physics,* 59th ed., pp. 78–79, CRC Press.
24. *Metal Reference Book* (Edited by C. J. Smithell) Butterworths, London (1976).
25. *Am. Inst. Physics Handbook,* 3rd ed. McGraw Hill (1972).
26. A. D. Brailsford and N. A. Gjostein, *J. appl. Phys.* **46,** 2390 (1975).
27. L. Holland, *Vacuum Deposition of Thin Films.* Chapman and Hall, London (1970).